Variation of momentum accommodation coefficients with pressure drop in a nanochannel

Sooraj K. Prabha [*] and Abdul Gafoor C. P.

Department of Mechanical Engineering, Vidya Academy of Science and Technology, Thrissur 680501, India

Sarith P. Sathian

Department of Applied Mechanics, Indian Institute of Technology Madras, Chennai 600036, India

Accommodation coefficients (ACs) are the phenomenological parameters used to evaluate gas-wall interactions. The gas transport through a finite length nanochannel will confront the variation of properties along the length of the channel. A three-dimensional molecular dynamics simulation has been carried out to examine this streamwise inhomogeneity of flow characteristics in a nanochannel. The rarefaction of the flow to the downstream direction is a crucial behavior in a pressure-driven nanochannel flow. This is manifested as the variation in velocity and temperature along the length of the channel. Subsequently, the interactions between the gas and wall particles will get reduced considerably. Moreover, the characteristics near the wall are examined in detail. A nonhomogeneous behavior in density and velocity profile near the wall is reported. Further, the momentum accommodation coefficient (MAC) in both the tangential and normal directions is examined along the lengthwise sections of the channel. The results show a significant variation of tangential and normal MACs along the length. Further, three channels with different length-to-characteristic dimension (L/H) ratios are considered to investigate the effect of L/H ratio. All three channels are subjected to the same pressure drop along the length. It is observed that the MACs and slip length show distinct behavior for different (L/H) ratios. The work establishes that the variation of MAC along the length of the channel has to be considered in modeling the nano- and microtransport systems.

I. INTRODUCTION

Nanoscale transport systems are gaining attention over the past decade in many fields such as nanofluidic systems, hybrid micro- and nanofluidic systems, and unconventional energy engineering. In nanofluidic systems, especially in gas flow systems, as the size decreases, the characteristic dimension of the system is comparable with the mean-free path (λ) of the gas molecules. Therefore, the flow field in these systems will no longer be in the continuum regime, but it could be in the slip or transition regime [1]. In these regimes of the flow, the gas-gas interactions will recede and gas-surface interactions will become more prevalent. Under such conditions, two distinct flow domains can be identified as (1) a bulk region at the center and (2) a near-wall region and thus arises an inhomogeneity in the perpendicular direction of the flow. As a result of this nonhomogeneous characteristic, many unexpected behaviors such as slip and incomplete accommodation have been reported [2,3]. Thus, nonhomogeneous fluid distribution in the system is a crucial characteristic of nanoscale transport.

Classical fluid transport theories do not account for these inhomogeneities, and transport parameters such as diffusivity and viscosity are strongly influenced by the fluid layering in nanochannels [4]. The deviations from the classical results are mainly due to the dominating effect of gas-surface interactions. As the gas-surface interactions become predominant, the analysis in the neighbourhood of the gas-surface interface becomes relevant [4–6].

Particle-based simulation methods are successful in capturing the real physics involved in gas-surface interactions. Methods such as molecular dynamics (MD) and direct simulation Monte Carlo (DSMC) can give fundamental insights into this. The use of several stochastic models are discussed in the literature to model the gas-wall interactions in the nanoscale conduits [7–11]. These models use one or more phenomenological parameters called accommodation coefficients (ACs), which represent the momentum and energy exchange between the gas and the solid surface. Consequently, these ACs are used to describe the gas-wall interactions in models such as Maxwell [11] and Cercignani-Lampis-Lord [10]. Over the years several different slip models have been used to extend the validity of the Navier-Stokes (NS) equation beyond the continuum regime. Likewise, an extension of the NS equation to transition flow regimes using an appropriate slip model is also reported in the literature [3,12,13]. In all these slip models the key input parameter is AC, and, therefore, the determination of ACs in various flow conditions is crucial in the modeling of nanoscale or hybrid micro- and nanoscale transport systems [13–15]. The ACs are very sensitive to many parameters (surface conditions, rarefaction, other thermophysical properties, etc.), and, consequently, the method to compute it requires careful handling [16–18].

_____
[*]sooraj.kp@vidyaacademy.ac.in

The tangential and normal momentum accommodation coefficients are defined as

$$\overline{\alpha_t} = \frac{p_i - p_o}{p_i}, \tag{1}$$

$$\overline{\alpha_n} = \frac{p_i - p_o}{p_i - p_T}, \tag{2}$$

where p is the momentum of gas particles. The subscripts denote whether the momenta should be calculated from the incident particles i, outgoing particles o, or the thermal wall T [16,19].

MD is considered as an appropriate method to determine ACs as it offers realistic modeling of a solid surface and the interactions among the particles [6,20]. Several studies report the determination of ACs using MD. In earlier studies, the attempt was to determine ACs of a stagnant gas bounded between the solid walls [16]. The determination of ACs for a binary gas mixture is also demonstrated in the literature [21]. It is also reported that the ACs determined from MD simulation are used to extend the validity of the NS equation to the transition regime with a higher second-order slip model [13]. The ACs determined using MD are further used in DSMC models for mesoscopic scale simulations [22]. Recently a statistical technique using a Gaussian mixture model is proposed based on data from molecular dynamics simulations [23]. The model is further validated for prediction of the velocity slip and temperature jump coefficients at the gas-solid interface. Apart from such studies, the dependence of accommodation coefficient on flow parameters is also examined in detail. The Knudsen number of the flow in a nanochannel predominantly affects the ACs [13]. Further, the effects of various factors like molecular mass, gas-surface interaction strength, and geometry of the channel on gas-surface interactions, and consequently of the the ACs, are investigated [24–26]. The effect of surface roughness on the accommodation coefficient is also studied using various techniques [27,28].

Most of the studies that focus on gas-surface interaction and determination of ACs use models with a streamwise homogeneous flow [5]. These models are not capable of capturing the flow characteristics in a pressure-driven flow, which is the driving mechanism of the flow in many applications. For instance, shale gas extraction involves flow through nanoscale pores where distinct pressure gradients exist in each pore along the length. Moreover, the variation of ACs at different length sections in a long channel is yet to be investigated.

To consider the streamwise inhomogeneity, the flow must be driven by a pressure gradient in the channel. Several methods were employed in the past to realize a pressure-driven flow in the channel. Dual-control-volume grand-canonical molecular dynamics is a widely accepted approach to induce a pressure gradient inside the channel [29]. In this method, the particles are inserted and deleted according to the reservoir condition, and hence, this method is computationally expensive. The reflecting particle membrane is another approach to establishing a pressure gradient inside the channel [30–32]. Further, a modified gravity-driven method is also used to model pressure-driven flow in a nanochannel in which the gravity is applied to a certain length at the entry of the channel [33]. In the present study, this method is used to model the pressure-driven gas flow in a finite length L channel.
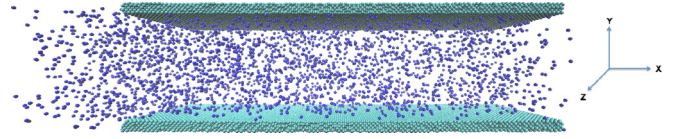

FIG. 1. An isometric view of the simulation domain. The fluid atoms are shown in blue.

From these discussions, it can be asserted that the ACs for a pressure-driven flow in a long channel are yet to be investigated. In this study is reported the variation of momentum accommodation coefficients (MACs) along the length of a nanochannel using MD. Three channels with different L/H ratios, where H is the characteristic dimension, are considered, and their effects on the MACs are analyzed at different locations of the channel. The results show that the rarefaction in downstream direction increases with an increase in L/H ratio, and the value of MACs decreases with an increase in pressure drop.

II. COMPUTATIONAL DETAILS

In this study, a three-dimensional model of rarefied gas (argon) flow confined between two parallel plates (platinum) is considered for simulation. The fluid atoms are initially configured randomly in between the solid walls. The dimensions of the simulation domain are chosen to be $50 \times (H + 2W) \times 10$ nm, where W is the thickness of the wall. An isometric view of the simulation domain is shown in Fig. 1 [34]. The direction of the flow is in the positive x direction, and the characteristic dimension (H) is in the y direction as shown in Fig. 1.

The total length of the simulation domain is divided into two: (1) the reservoir portion and (2) the channel section of length $L = 40$ nm. A gravity is applied to the gas molecules in the positive x direction at the entry of the reservoir. Therefore, the gas molecules present in the rest of the reservoir and the channel region are kept completely undisturbed. Thus, the flow is driven solely by the pressure gradient developed across the channel.

The interactions between the atoms in the system are modeled by a Lennard-Jones (LJ) pairwise potential field, which is defined as

$$U_{ij}(r_{ij}) = 4\,\varepsilon_{ij}\left[\left(\frac{\sigma_{ij}}{r_{ij}}\right)^{12} - \left(\frac{\sigma_{ij}}{r_{ij}}\right)^{6}\right], \tag{3}$$

where r_{ij}, ε_{ij}, and σ_{ij} are the distance between two atoms, interaction strength, and LJ length parameter, respectively. The values of these LJ parameters used for the simulation are given in Table I. The length parameter for Ar-Pt interaction

TABLE I. Parameters used for the LJ interaction potentials.

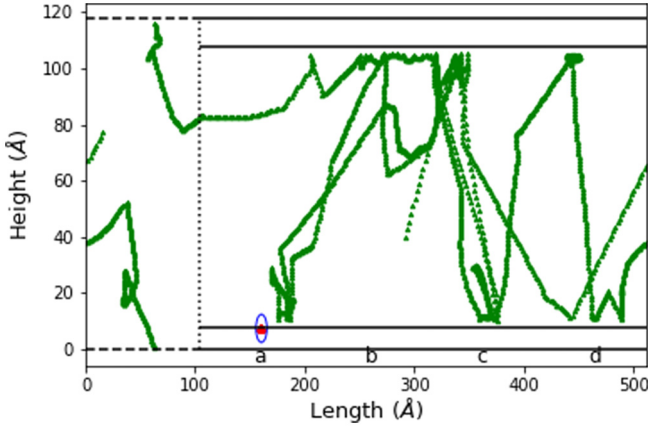| Interactions	ε (eV)	σ (nm)
Ar-Ar	0.01029	0.341
Ar-Pt	0.00682	0.294
Pt-Pt	0.32501	0.247

FIG. 2. Molecular trajectory of a single gas atom and a wall atom. The vertical dotted line represents the entry of the channel section. The dashed lines represent the system boundaries. *a, b, c,* and *d* represent the position of the bins.

($\sigma_{\text{Ar-Pt}}$) is calculated from the Lorentz-Berthelot mixing rule as $(\sigma_{\text{Ar}} + \sigma_{\text{Pt}})/2$. The energy interaction strength parameter $\varepsilon_{\text{Ar-Pt}}$ is borrowed from the literature [16].

The cutoff distance σ_c is taken as 2.5 times the LJ length parameter (σ). The MD movements of the particles are calculated with a time step of 1 fs, and the total production run is for 8–10 ns. The wall is maintained at 400 K using a Berendsen thermostat [35].

III. RESULTS AND DISCUSSIONS

In this study, the average rarefaction levels inside the channel are maintained at a value of Knudsen number (Kn = λ/H) 0.30 $\pm$ 0.03. The total channel length is divided into four bins marked as *a, b, c,* and *d* as shown in Fig. 2. The properties in each bin are calculated by averaging the individual properties over the bin volume. The variation of properties for different L/H ratios is studied by varying the characteristic dimension H, keeping the average Knudsen number a constant. The height of the channel H is varied from 6 nm to 10 nm.

A. Molecular trajectories

The stability of the model is one of the issues of concern in simulating flow through relatively long channels. To examine the structural stability of the MD model, randomly selected gas and wall atoms are tracked for a finite number of time steps. Figure 2 shows the trajectories of these two atoms in two-dimensional (xy) coordinates. The continuous lines in the figure represent the wall boundaries, and the dotted vertical line represents the entry of the channel section. The points (green) show the path traced by the gas atom. It can be seen that it executes random as well as directional movements between the wall boundaries. On the other hand, the wall atom (circled for easy reference) maintains its mean position over time, which indicates the structural integrity of the wall during the simulation.
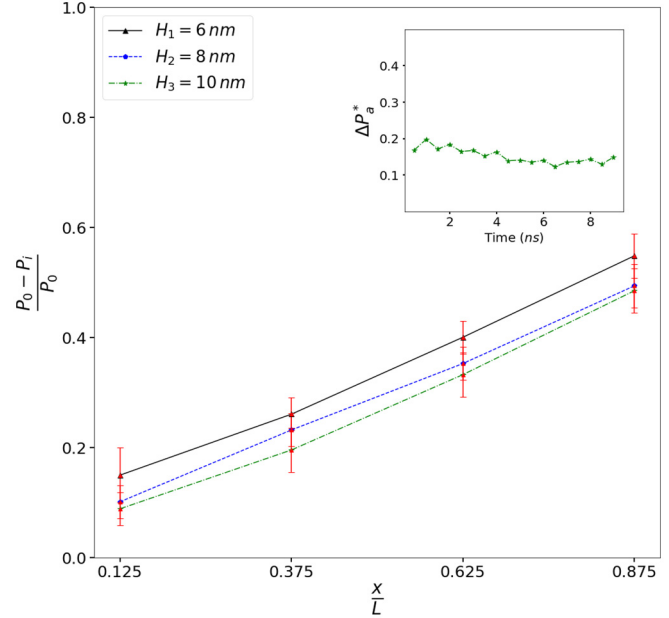

FIG. 3. The pressure drop ΔP_i^* shows a linear variation with the normalized length. The pressure drop is normalized with the P_0, the pressure at the reservoir. The inset shows the pressure drop at first bin *a* of the 6 nm channel over a finite simulation period.

B. Pressure drop

To portray the variation of pressure drop along the length of the channel, the pressure in each bin P_i is determined. The normalized pressure drop is plotted against the normalized length parameter as shown in Fig. 3. The normalized pressure drop in each bin is calculated as $\Delta P_i^* = (P_0 - P_i)/P_0$, where P_i is the pressure at the respective bin and P_0 is the pressure at the reservoir. As seen in the figure, the pressure drop ΔP_i^* shows a linear variation with the length parameter. It shows a similar variation for all the three cases. The attempt was to maintain a constant pressure drop for each channel, and the average pressure drop across the channel is obtained as 0.45 $\pm$ 0.03. To analyze the system at a definite pressure drop, the system has to maintain the characteristics throughout the simulation. The inset figure shows the pressure drop in a bin of the channel. The P_a^* is varying within a narrow limit throughout the simulation period, which indicates a stabilized flow.

C. Velocity and temperature

The pressure drop in the channel will influence the thermophysical properties along the length. To elucidate this, the variation of velocity and temperature along the channel length is plotted as shown in Fig. 4. These properties are normalized with the corresponding values in the reservoir. As seen in the figure, an increase in velocity is observed in the downstream direction of the system. Meanwhile, a decrease in temperature is observed in the flow direction, and the change in temperature is nominal at the downstream. These are the characteristics of a typical nanoscale pressure-driven flow.
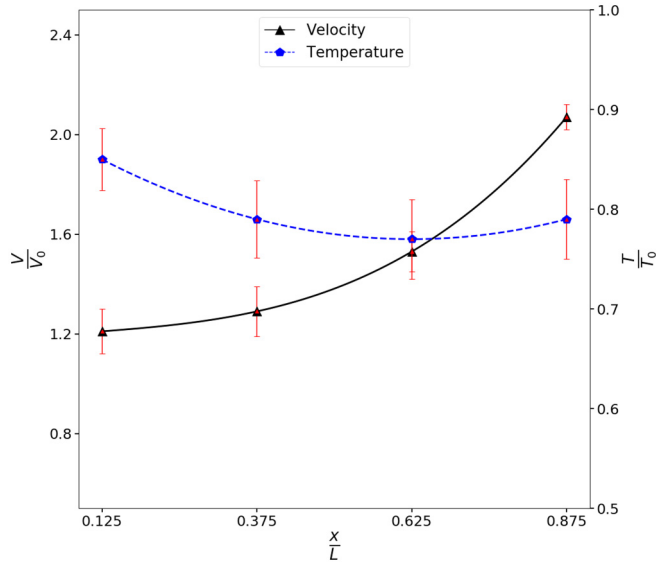
FIG. 4. The velocity increases along the length of the channel whereas the temperature decreases and the variation in the temperature is nominal at the downstream. The velocity and temperature are normalized with the corresponding values at the reservoir. The plots for a 6 nm channel are shown.

D. Density and velocity profiles

For flows through nanoscale conduits, there will be density accumulation near the wall region due to the presence of strong potential fields. As reported in earlier studies, an increase in the density near the wall is observed as the flow proceeds towards the downstream (Fig. 5). This local accumulation near the wall leads to a corresponding reduction in the bulk region. Another significant parameter near the wall
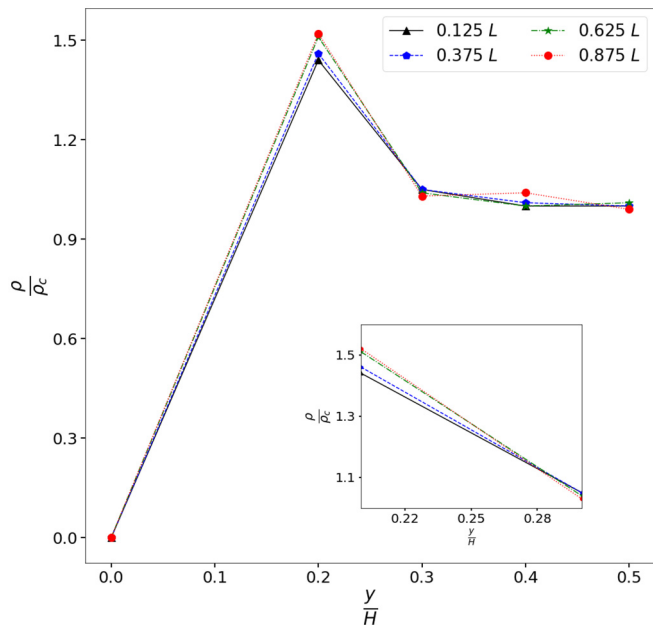

FIG. 5. The density profiles across the nanochannel at the respective bins. The local density is normalized with the center line density. Only half of the channel section is shown.
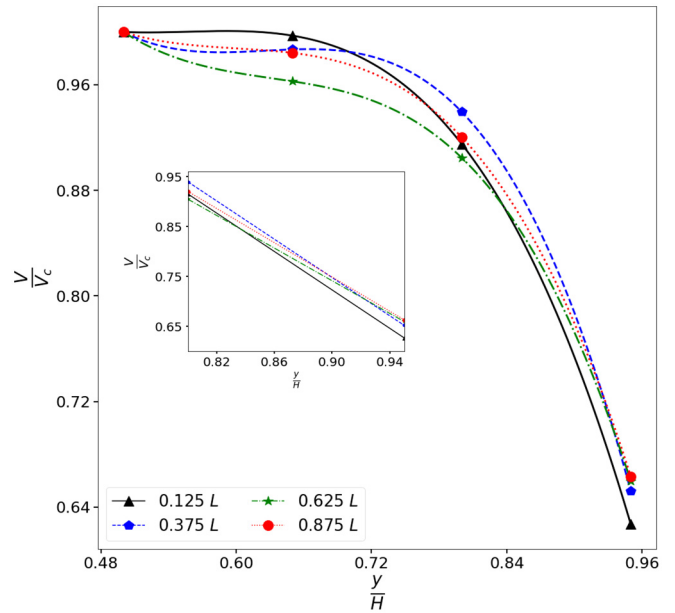

FIG. 6. The velocity profile across the nanochannel is shown. The local velocity is normalized with the center line velocity. The extreme points near the wall indicate the amount of slip. Only half of the channel section is shown.

region is the slip velocity. A qualitative assessment of slip phenomenon can be observed from the velocity profiles across the channel. To illustrate this clearly, the velocity across the flow is depicted in Fig. 6. It is expected that rarefaction levels will increase down the channel. This is evident from the near-wall velocity that increases along the length. Furthermore, the normalized velocity profile near the wall also flattens as the flow proceeds downstream.

These results clearly show the nature of a typical rarefied gas flow in the nanoscale conduit. Thus, the present model is capable of simulating the characteristics of the nanoscale pressure-driven flows, and the nature of momentum accommodation coefficients is studied using this stabilized simulation model with the same set of parameters. In the following, we will examine the calculated values of MAC and its variation along the length of the channel.

E. Accommodation coefficients

To calculate ACs [Eqs. (1) and (2)], incoming and outgoing velocities of gas atoms after every collision with the wall are recorded. In the present model, a virtual plane is placed near the wall at a distance of 2.5 σ_{Ar-Pt}, where σ_{Ar-Pt} is the LJ length parameter for fluid-wall interaction. When the atom is moving towards the wall, incident components are logged, and when the atom is moving away from the wall, the reflected components are logged and these two comprise a collision [16,36]. The accuracy of the MACs thus calculated depends on the number of independent collisions recorded.

1. Tangential momentum accommodation coefficients

To calculate TMAC, the incident component of velocity is always taken as positive, and if the direction changes upon
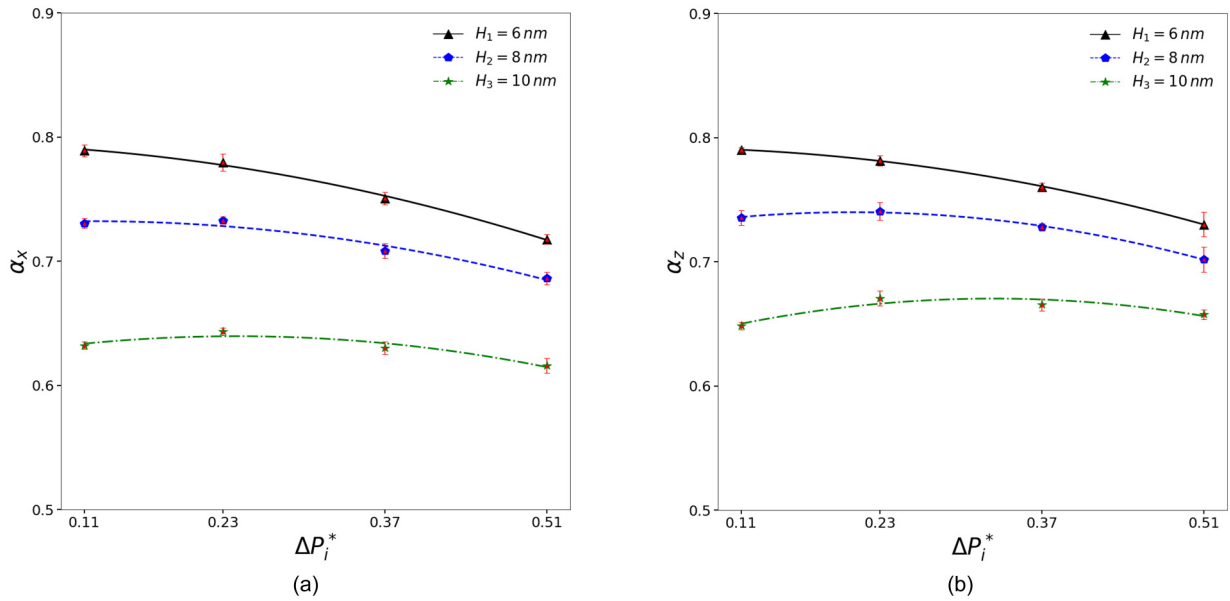
FIG. 7. Variation of tangential momentum accommodation with the normalized pressure drop and H. As the solid surface is in xz plane it will have two tangential components, the momentum accommodation in the x and z directions [7(a) and 7(b)].

collision, the reflected component is taken as negative. The tangential MACs thus calculated from the collision data are plotted against the normalized pressure drop as shown in Fig. 7. As the high rarefaction in the downstream reduces the gas-surface interactions, it can be noted that a lower TMAC is obtained in the downstream. Further, a decrease in channel characteristic height H escalates the frequency of the collisions in the channel. As a result, an increase in TMAC can be observed as the H decreases (Fig. 7).

The high rarefaction in the downstream reduces the gas-surface interactions. Moreover, a high slip velocity, as the flow proceeds, causes a reduction of the interaction time. It can be noted that a lower TMAC is obtained in the downstream and it is decreasing monotonically. This reaffirms the fact that the ACs are highly dependent on the rarefaction levels. These variations of TMAC in different length sections influence the flow characteristics in the channel.

2. Normal momentum accommodation coefficients

The absolute values of the normal component of velocities are taken for the calculation of the normal momentum accommodation coefficient (NMAC) [Eq. (2)] and plotted against the normalized pressure drop in Fig. 8. As the NMAC depends on the wall temperature, a lower value of NMAC is expected as compared with the TMAC. Further, the NMAC shows a reverse trend compared to TMAC when the H varies. As the H decreases the local transport of gas atoms in y direction reduces.

F. Slip length

The slip length is another parameter that describes the rarefied flows in a nanochannel. As the local values of α_x and Kn vary along the streaming direction, it will be interesting to study the variation of slip length. According to Maxwell's model, the dimensionless slip length is related to the Knudsen number as $l_{sM} = [(2 - \alpha_x)/\alpha_x]$ Kn. The calculated values of TMAC (α_x) are used to determine the slip length at different locations along the length of the channel (Fig. 9). It increases with an increase in pressure drop, and it decreases with a decrease in the characteristic dimension. It is reported in the literature that the l_{sM} shows a linear relationship with the Knudsen number for short channel lengths [13]. However, a nonlinear variation of slip length is observed in Fig. 9, where the pressure drop in the channel becomes significant. This information is helpful in fine-tuning the thermophysical property calculations in nanoscale transport.
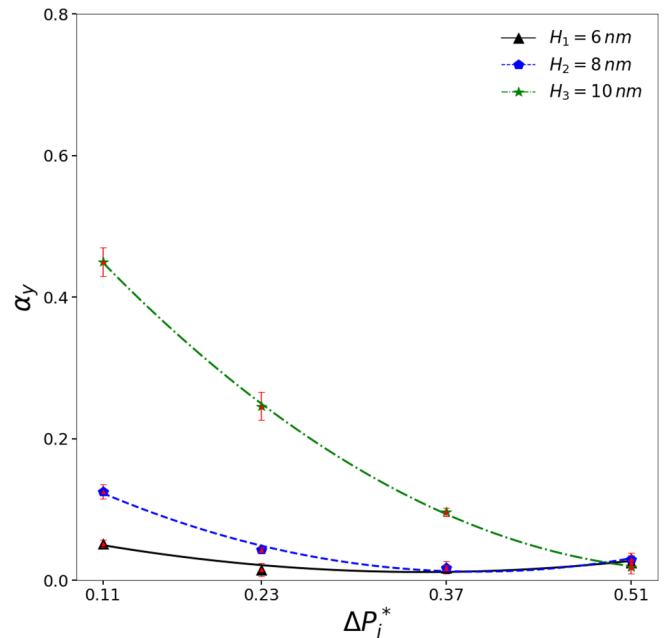

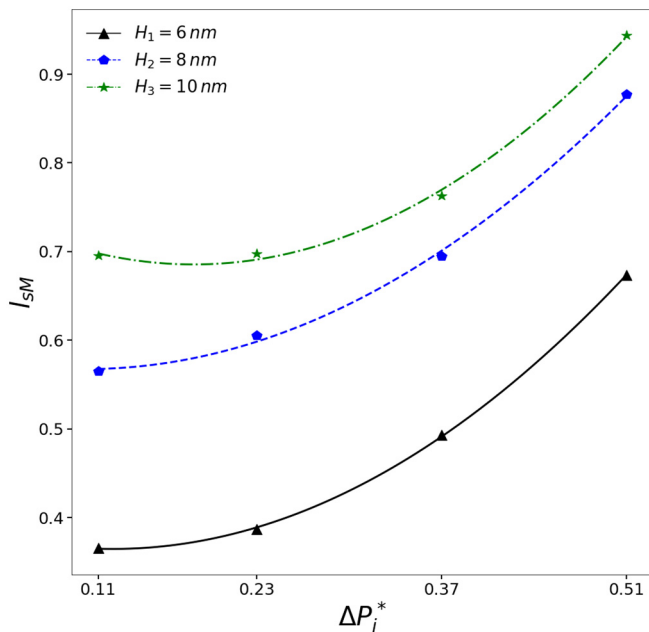FIG. 8. Variation of normal momentum accommodation (NMAC) with the normalized pressure drop and H.

FIG. 9. The variation of Maxwell's slip length l_{sM} with the normalized pressure drop for different channel height H. The slip length is obtained from the calculated values of TMAC.

of the channel is observed. This characteristic is exemplified by the variation in velocity and temperature along the length of the channel. Moreover, the characteristic near the wall is so crucial in nanoscale flows. The near-wall density and velocity profiles show an increase near the wall region, and it depicts a typical characteristic of a rarefied flow. Further, the variation of the properties with respect to the L/H ratios of the channel is also investigated.

To study the gas-surface interactions in detail, MACs are determined at various locations in the channel. A monotonic decrease in MACs is found in all three cases along the flow direction. Further, the dependence of MACs on L/H ratio is also analyzed. A higher value of TMAC is reported for channels with a smaller characteristic dimension H. The variation in ACs in the tangential and normal direction shows distinct behavior with respect to the H of the channel. Therefore, the analytical models for the analysis of nanoscale transport must consider the variation of MAC with pressure drop for the accurate prediction of properties. The TMAC in the flow direction is used to study the slip length using Maxwell's model. Though the model suggests a linear relationship between slip length and Knudsen number, a nonlinear variation is observed along the length. Hence it can be concluded that the flow characteristics in a system with a constant pressure drop can exhibit a nonlinear variation.

IV. CONCLUSION

A three-dimensional molecular dynamics study of a pressure-driven nanochannel flow has been conducted to study the streamwise inhomogeneity of the flow characteristics. The development of higher rarefaction towards the downstream

ACKNOWLEDGMENTS

[1] S. Colin, *Microfluidics* (John Wiley & Sons, New Jersey, 2013).

[2] L. Bocquet, Nat. Mater. **19**, 254 (2020).

[3] W.-M. Zhang, G. Meng, and X. Wei, Microfluid. Nanofluid. **13**, 845 (2012).

[4] G. Karniadakis, A. Beskok, and N. Aluru, *Microflows and Nanoflows: Fundamentals and Simulation*, Interdisciplinary Applied Mathematics Vol. 29 (Springer Science & Business Media, New York, 2006).

[5] C. Huang, P. Y. Choi, and L. W. Kostiuk, Phys. Chem. Chem. Phys. **13**, 20750 (2011).

[6] R. B. Schoch, J. Han, and P. Renaud, Rev. Mod. Phys. **80**, 839 (2008).

[7] A. Tenenbaum, G. Ciccotti, and R. Gallico, Phys. Rev. A **25**, 2778 (1982).

[8] R. Tehver, F. Toigo, J. Koplik, and J. R. Banavar, Phys. Rev. E **57**, R17 (1998).

[9] K. Yamamoto, H. Takeuchi, and T. Hyakutake, Phys. Fluids **18**, 046103 (2006).

[10] C. Cercignani and M. Lampis, Transp. Theory Stat. Phys. **1**, 101 (1971).

[11] J. C. Maxwell, Philos. Trans. R. Soc. London **170**, 231 (1879).

[12] B.-Y. Cao, M. Chen, and Z.-Y. Guo, Phys. Rev. E **74**, 066311 (2006).

[13] S. K. Prabha and S. P. Sathian, Phys. Rev. E **85**, 041201 (2012).

[14] S. Nedea, A. Markvoort, A. van Steenhoven, and P. Hilbers, in *ASME 2007 5th International Conference on Nanochannels, Microchannels, and Minichannels* (American Society of Mechanical Engineers Digital Collection, Puebla, Mexico, 2007), pp. 755–762.

[15] J. Sun and Z.-X. Li, Mol. Simul. **35**, 228 (2009).

[16] P. Spijker, A. J. Markvoort, S. V. Nedea, and P. A. J. Hilbers, Phys. Rev. E **81**, 011203 (2010).

[17] P. Spijker, A. J. Markvoort, P. A. Hilbers, and S. V. Nedea, AIP Conf. Proc. **1084**, 659 (2008).

[18] B.-Y. Cao, J. Sun, M. Chen, and Z.-Y. Guo, Int. J. Mol. Sci. **10**, 4638 (2009).

[19] S. R. Cook and M. A. Hoffbauer, Phys. Rev. E **58**, 504 (1998).

[20] Q. D. To, T. T. Pham, G. Lauriat, and C. Léonard, Adv. Mech. Eng. **4**, 580763 (2012).

[21] S. K. Prabha and S. P. Sathian, Microfluid. Nanofluid. **13**, 883 (2012).

[22] S. A. Peddakotla, K. K. Kammara, and R. Kumar, Microfluid. Nanofluid. **23**, 79 (2019).

[23] M. Liao, Q.-D. To, C. Léonard, and W. Yang, Phys. Rev. E **98**, 042104 (2018).

[24] J. Kim, A. J. Frijns, S. V. Nedea, and A. A. van Steenhoven, Microfluid. Nanofluid. **15**, 661 (2013).

[25] H. Yamaguchi, Y. Matsuda, and T. Niimi, Phys. Rev. E **96**, 013116 (2017).

[26] T. Acharya, J. Falgoust, I. Schoegl, and M. J. Martin, J. Thermophys. Heat Transfer **33**, 773 (2019).

[27] B.-Y. Cao, M. Chen, and Z.-Y. Guo, Int. J. Eng. Sci. **44**, 927 (2006).

[28] K. K. Kammara, R. Kumar, A. K. Singh, and A. K. Chinnappan, Phys. Rev. Fluids **4**, 123401 (2019).

[29] A. P. Thompson, D. M. Ford, and G. S. Heffelfinger, J. Chem. Phys. **109**, 6406 (1998).

[30] J. Li, D. Liao, and S. Yip, Phys. Rev. E **57**, 7259 (1998).

[31] F. Bao, Y. Huang, Y. Zhang, and J. Lin, Microfluid. Nanofluid. **18**, 1075 (2015).

[32] F. Bao, Y. Huang, L. Qiu, and J. Lin, Mol. Phys. **113**, 561 (2015).

[33] M. Kazemi and A. Takbiri-Borujeni, J. Nat. Gas Sci. Eng. **33**, 1087 (2016).

[34] W. Humphrey, A. Dalke, and K. Schulten, J. Mol. Graphics **14**, 33 (1996).

[35] H. J. Berendsen, J. v. Postma, W. F. van Gunsteren, A. DiNola, and J. Haak, J. Chem. Phys. **81**, 3684 (1984).

[36] S. K. Prabha and S. P. Sathian, Int. J. Therm. Sci. **81**, 52 (2014).